Analytical and finite element modelling of long plate mode jumping behaviour

Thin-Walled Structures 73 (2013) 101–111

Contents lists available at ScienceDirect

Thin-Walled Structures

journal homepage: www.elsevier.com/locate/tws

Analytical and finite element modelling of long plate mode jumping behaviour

H. Hofmeyer *, J. Courage

Technische Universiteit Eindhoven, Department of the Built Environment, Structural Design Group, VRT 9.32, P.O. Box 513, 5600 MB Eindhoven, The Netherlands

ARTICLE INFO

Article history:
Received 20 December 2012
Received in revised form
24 June 2013
Accepted 25 June 2013

Keywords:
Mode Jumping
Analytical Modelling
Finite Element Modelling

ABSTRACT

Trapezoidal sheeting of thin-walled steel is applied frequently for roofing and cladding. As such, it is loaded by a concentrated load (at the support) and a bending moment. A recently developed model to predict the sheeting's failure behaviour leaves the question open whether mode jumping (the phenomenon where a plate dynamically changes its buckling mode during an increasing load) should be taken into account in the model. This article presents the analytical and finite element modelling of square and long plates, which, depending on the boundary conditions, may represent the compressed flange of trapezoidal sheeting. The analytical modelling is based on the combination of several displacement functions and using the principle of minimal potential energy. Hereafter the stability of each part of the resulting equilibrium curves is determined. A spin-off of the analytical model is an analytical expression for a current curve-fitted based prediction formula for the post/pre-buckling stiffness ratio by Rhodes. Furthermore, the accuracy range of a solution by Williams and Walker for the far-post buckling behaviour can be confirmed. The finite element modelling has been carried out by implicit dynamic, and explicit (dynamic) simulations. Both for the load levels and the buckling mode sequences, the analytical and finite element models give equivalent results. It is concluded that for the specific boundary conditions that represent the situation of a compressed flange for trapezoidal sheeting, it is very likely that mode jumping will not occur.

1. Introduction

Sheeting of thin-walled steel is widely used for the construction of building roofs and claddings. Near the intermediate supports, which are either hot-rolled steel beams or cold-formed sections, the sheeting is loaded by a combination of bending moment due to distributed loads on the sheeting and a concentrated load due to the support reaction, Fig. 1a.

Either mainly the concentrated load leads to failure via so-called web-crippling [1–5], or the combination of web-crippling and bending moment may induce failure [6–12]. Current design codes [13,14] predict failure due to this latter load combination as follows. First, the ultimate bending moment M_u that the sheeting can withstand is predicted without taking the action of the concentrated load F into account. This prediction is carried out by the semi-analytical effective width method which is based on the work of Von Kármán [15] for very slender plates and the additional work of Winter [16] for plates with a slenderness normally used in sections of cold-formed steel. The North American and Australian specifications also allow the use of the direct strength method [17,18] as an alternative to the effective width method. For this method, not the separate compressed elements, but the whole cross-section is analysed for local, global, and distortional buckling, resulting in the critical bending moment. The ultimate bending moment can then be found by curve-fitting the relationship between critical moment, normalised with the moment of first yield, and the ultimate bending moment, also normalised. Secondly, the design codes require the prediction of the ultimate concentrated load R_w, defined as web-crippling load, without taking the effect of the bending moment M into account. This prediction of R_w is purely based on curve-fitting of test-results [19–38]. Finally, sheeting failure by a combination of bending moment and concentrated load is predicted by an interaction rule, as shown in Fig. 1b, which is also purely based on curve-fitting of test-results [19,21,39–42]. The ultimate corresponding reaction load on the section is defined as load F_u.

Fig. 1b clearly shows that the procedure in the current design codes is a combination of several procedures, both semi-analytical and curve-fitting, and it is not based directly on the occurring failure modes. Therefore, the ultimate failure model was developed [43], conceptually presented in Fig. 2 showing a part of the compressed flange.

* Tel.: +31 40 247 2203.
E-mail address: h.hofmeyer@bwk.tue.nl (H. Hofmeyer).

0263-8231/$ - see front matter © 2013 Elsevier Ltd. All rights reserved.
http://dx.doi.org/10.1016/j.tws.2013.06.017

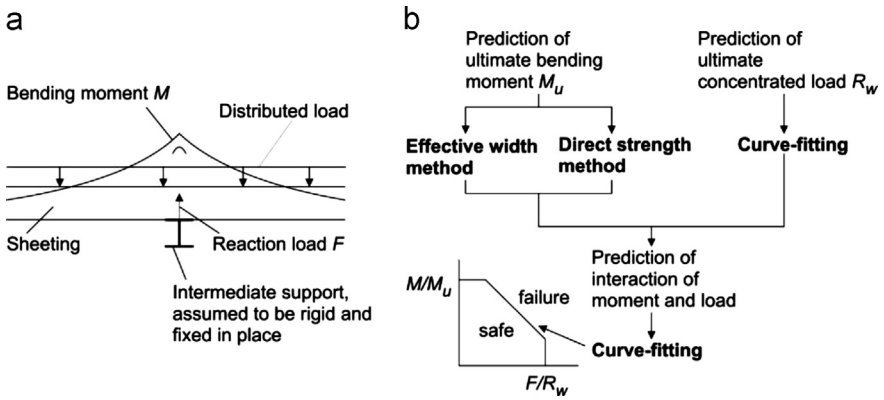

Fig. 1. (a) Sheeting loaded by combination of moment and force and (b) current design codes.

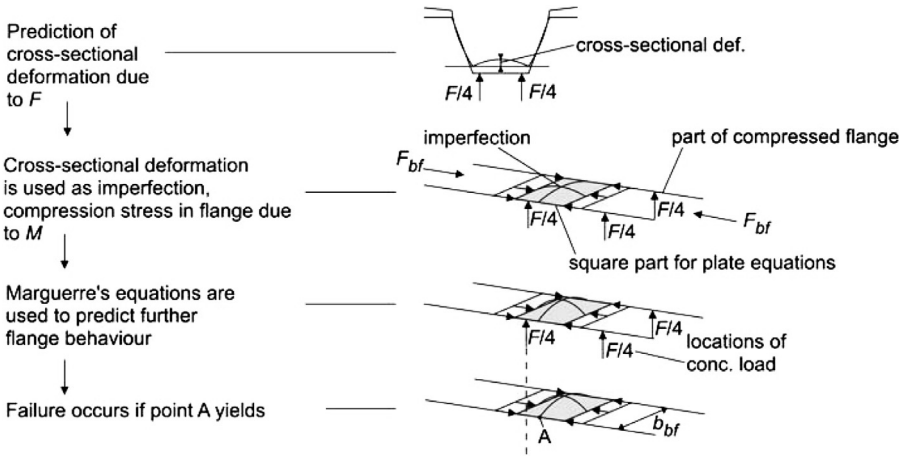

Fig. 2. Concept of ultimate failure model.

Experiments [43] showed that the elastic deformation of the compressed flange was always such that the relevant part of it could be modelled by a square element, shown shaded in Fig. 2, starting at a distance of 0.25 times the flange width to the concentrated load application. The concentrated load F on the sheeting is modelled as four point loads $F/4$. Due to these four point loads, the cross-section deforms and as a result the compressed flange shows an out-of-plane deflection. Besides this effect, the concentrated load F also causes a bending moment M on the sheeting. This bending moment causes a compression force F_{bf} in the flange that can be made equivalent to a certain average compression stress in the flange. Now, Marguerre's [44] equations are used to determine the (initial post-buckling) plate behaviour for the initial imperfection (that is the out-of-plane deflection caused by the concentrated load) and the compressive stress caused by the bending moment. As soon as the outer-fibre stress in point A is such that the yielding stress is reached, the sheeting is assumed to fail. Note that the action of the concentrated load is taken into account only indirectly, via the cross-sectional deformation and the compression stresses due to the bending moment, and that local additional stresses at A directly due to the concentrated load are not incorporated.

This ultimate failure model performs well compared to current design codes; however, the plate equations of Marguerre have three disadvantages. First of all they are too tedious to use as a design rule. Secondly, they are only able to predict failure by first yield of a single location in the plate. However, research has shown that the failure of a compressed plate can occur in two different modes and for these modes, first yield is not always a good predictor of the ultimate load [45]. Finally, they are only valid for the initial post-buckling behaviour (loads up to about two times the buckling load) in which it is assumed that the displacement fields before and after buckling are the same. Therefore, the fictitious strain method has been developed, which replaces Marguerre's equations, is easier to use, is also suitable for far post-buckling behaviour, and provides additional insight into the plate failure behaviour [45]. The fictitious strain method has already been used and discussed in literature [46–50].

The ultimate failure model, preferably used in combination with the fictitious strain method instead of Marguerre's equations, is not suitable for second-generation sheeting, which is sheeting with longitudinal stiffeners. This is the case because the fictitious strain method (and also Marguerre's equations) had been developed for first-generation sheeting, which is sheeting with flat plates only. Therefore research was started on the application of the fictitious strain method on second-generation sheeting, thus on plates with longitudinal stiffeners [51]. Using the finite element method for this research, it came out that plates with longitudinal stiffeners could only be modelled as long plates, instead of the computationally more efficient square plates as used for flat plates. But even before these plates with longitudinal stiffeners were simulated, instabilities occurred in the finite element analyses for the flat long plates and it was thought that among these instabilities also mode-jumping phenomena existed [51]. This was regarded as a serious drawback as mode jumping phenomena would undermine the principles of the fictitious strain method. Therefore a new research project was initiated, presented here, in which the mode jumping phenomena was investigated in more detail. Besides a new analytical approach to model mode jumping behaviour analytically, the finite element models used indicated

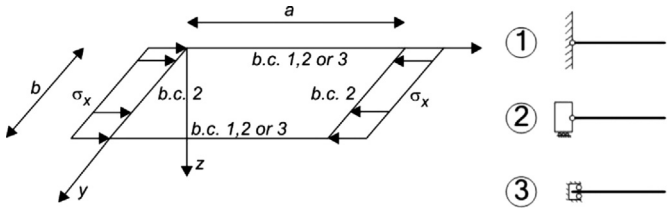

Fig. 3. Perfect plate, compressed in one direction, and several possible boundary conditions.

that trapezoidal sheeting is not prone to mode jumping phenomena, at least for first-generation sheeting. This ensures that the ultimate failure model in combination with the fictitious strain method can be used.

In this article, Section 2 will give a brief overview on plate buckling, which makes it possible to present the approach on modelling the post-buckling behaviour of plates in Section 3. Section 4 will present mode jumping phenomena, both by means of the approach presented in Section 3 and by means of finite element models. Discussion and conclusions can then be found in Section 5.

2. Buckling behaviour

A plate is studied as shown in Fig. 3. All edges are simply supported, which means no displacements normal to the plate surface are allowed and rotations around the edge line are free. With respect to in-plane behaviour, the loaded edges should remain straight (b.c. 2) and to start, it is assumed that the unloaded edges are straight but allowed to displace (b.c. 2) or able to wave in-plane (b.c. 3). Edges that remain straight and are not allowed to displace (b.c. 1) will be treated later. If the plate would be perfectly flat and would contain no other possible imperfections, it would remain flat until the buckling load, at which it would buckle out-of-plane only if an (even very small) irregularity in the boundary conditions or geometry would occur. This is defined here as bifurcation buckling. In practice, however, small imperfections will always exist, leading to out-of-plane deflections directly after the start of loading, and this behaviour is defined here as geometrical non-linear buckling. In this section, as an introduction to more complex theories, a brief overview on the determination of the bifurcation load of the simple plate as shown in Fig. 3 will be presented. More detailed information can be found in e.g. Timoshenko [52].

First of all, equilibrium is determined for a small piece *dx–dy* of the plate. The fact that this equilibrium is defined for the plate having a deflected geometry means that internal normal forces may result in internal bending moments, due to uneven deflection of the piece *dx–dy,* and as such a stability calculation may follow. The equilibrium equation can be expressed entirely in stresses by means of linearised constitutive and kinematical equations:

$$D\nabla^4 w - t\left\{\frac{\partial^2\Phi}{\partial x^2}\frac{\partial^2 w}{\partial y^2} - 2\frac{\partial^2\Phi}{\partial x\partial y}\frac{\partial^2 w}{\partial x\partial y} + \frac{\partial^2\Phi}{\partial y^2}\frac{\partial^2 w}{\partial x^2}\right\} - Y = 0 \tag{1}$$

in which $w(x,y)$ is the deflection of the plate, t the thickness, D is the flexural rigidity of the plate (explained below), Y the distributed load, and Φ is a so-called Airy stress function that simplifies the solution of the differential equations

$$\sigma_x = \frac{\partial^2\Phi}{\partial y^2},\ \sigma_y = \frac{\partial^2\Phi}{\partial x^2},\ \tau_{xy} = \frac{\partial^2\Phi}{\partial x\partial y} \tag{2}$$

$$D = \frac{Et^3}{12(1-\nu^2)} \tag{3}$$

in which E is Young's modulus and υ is Poisson's ratio.

Strains and displacements are related by kinematic equations. By rewriting these kinematical equations, a relationship between the strains can be found, the so-called compatibility equation, which can again be expressed in stresses by using linearised constitutive equations:

$$\nabla^4\Phi = 0 \tag{4}$$

A plate should satisfy both the equilibrium and the compatibility equation. Note that if loads are uniformly distributed along the edges, the compatibility equation (Eq. (4)) is automatically satisfied (this will not be the case anymore once a second-order compatibility equation will be used in Section 3):

$$\nabla^4\Phi = \frac{\partial^4\Phi}{\partial x^4} + \frac{\partial^4\Phi}{\partial x^2 y^2} + \frac{\partial^4\Phi}{\partial y^4} = \frac{\partial^2\sigma_y}{\partial x^2} + \frac{\partial^2\tau_{xy}}{\partial xy} + \frac{\partial^2\sigma_x}{\partial y^2} = 0 + 0 + 0 \tag{5}$$

Because for the plate shown in Fig. 3 no normal load in y-direction or shear load is applied, the corresponding components in Eq. (1) can be removed:

$$D\nabla^4 w - t\frac{\partial^2\Phi}{\partial y^2}\frac{\partial^2 w}{\partial x^2} = D\nabla^4 w - t\sigma_x\frac{\partial^2 w}{\partial x^2} = 0 \tag{6}$$

A proposed solution for the differential equation above equals

$$w(x,y) = C\sin\left(\frac{m\pi x}{a}\right)\sin\left(\frac{n\pi y}{b}\right) \tag{7}$$

with C a constant, m and n being the number of half-waves along the plate, and a and b the length and width of the plate respectively as also shown in Fig. 3. It can be shown that this solution satisfies both the kinematic (Eq. (8)) and dynamic boundary conditions (Eq. (9), of which the derivations are elaborated in [52], page 321):

$$w(0,y) = w(a,y) = w(x,0) = w(x,b) = 0 \tag{8}$$

$$M_{x=0,a} = -D\left\{\frac{\partial^2 w}{\partial x^2} + \nu\frac{\partial^2 w}{\partial y^2}\right\}_{x=0,a} = 0,$$
$$M_{y=0,b} = -D\left\{\frac{\partial^2 w}{\partial y^2} + \nu\frac{\partial^2 w}{\partial x^2}\right\}_{y=0,b} = 0 \tag{9}$$

As such, once these are substituted in the differential Eq. (6), the exact buckling load $\sigma_{x;cr}$ is found by stating that the trivial solution is not relevant ($C\neq 0$), and finding n and m values for which the lowest stress in x-direction results:

$$\sigma_{x;cr;bc2,3} = \frac{\pi^2 D}{b^2 t}\left(m\frac{b}{a} + \frac{n^2 a}{mb}\right)^2 = \frac{\pi^2 D}{b^2 t}K_{mn} \tag{10}$$

So far, as mentioned, only b.c. 2 and 3 of the unloaded edges were taken into account. If the unloaded edges of the plate are straight and are not allowed to displace in-plane (b.c. 1 in Fig. 3), the boundary conditions are different and will yield a buckling load equal to

$$\sigma_{x;cr;bc1} = \frac{\pi^2 D}{b^2 t}K_{mn}\frac{1}{(1+(a^2/b^2)\nu)} \tag{11}$$

In Fig. 4 the coefficient K_{mn}, as defined in Eq. (10), is plotted against the a/b ratio and for $n=1$ and $m=1$, 2, 3, 4, or 5. Although this plot is purely meant for small deflections and initial values of a/b, it may be read as suggesting that for even slightly changing a/b ratios, for instance due to large deformations, other buckling modes could become dominant, thus making the phenomenon of mode-jumping more understandable. In Section 4 this suggestion will be checked and elaborated.

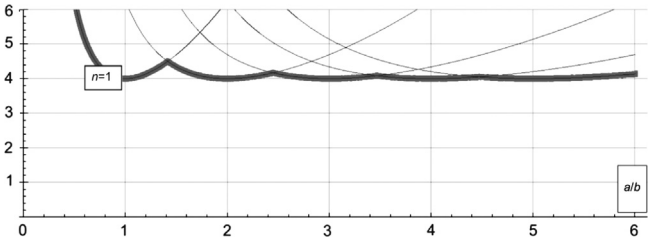

Fig. 4. Buckling coefficient K_{mn} as a function of the plate aspect ratio a/b.

3. Post-buckling behaviour

In the previous section only a buckling load value has been derived, which is a theoretical value for a perfect plate. In reality, a plate will always have imperfections and, even more important, especially for small imperfections, will have a clearly distinguishable difference in effective stiffness before and after the theoretical buckling load. In this Section 3, plate behaviour after buckling will be derived for two cases. For loads up to twice the buckling load, it can be assumed that the buckled shape will not change and this so-called "initial" post-buckling behaviour will be described in Section 3.1. For larger loads, the "far" post-buckling behaviour will be described in Section 3.2. The latter description will be used in Section 4 to theoretically predict mode-jumping behaviour.

3.1. Elastic, initial post-buckling behaviour

To describe initial post-buckling behaviour, in contrast to predicting the buckling load, it is now taken into account that (1) the total out-of-plane deflections $w(x,y)$ contain imperfections $w_0(x,y)$ and (2) the total deflections are so large that resulting strains should be taken into account, at least, in the mid-surface of the plate. All other assumptions are unchanged. This leads to a slightly modified equilibrium equation compared to Eq. (1) – only different in taking the imperfection into account – and a more extended compatibility equation compared to Eq. (4), due to taking into account the effect of out-of-plane deflections on in-plane normal and shear strains [44]:

$$D\nabla^4(w-w_0)-t\left\{\frac{\partial^2\Phi}{\partial x^2}\frac{\partial^2 w}{\partial y^2}-2\frac{\partial^2\Phi}{\partial x\partial y}\frac{\partial^2 w}{\partial x\partial y}+\frac{\partial^2\Phi}{\partial y^2}\frac{\partial^2 w}{\partial x^2}\right\}-Y=0 \tag{12}$$

$$\nabla^4\Phi+E\left\{\frac{\partial^2 w}{\partial y^2}\frac{\partial^2 w}{\partial x^2}-\left(\frac{\partial^2 w}{\partial x\partial y}\right)^2-\left(\frac{\partial^2 w_0}{\partial y^2}\frac{\partial^2 w_0}{\partial x^2}-\left(\frac{\partial^2 w_0}{\partial x\partial y}\right)^2\right)\right\}=0 \tag{13}$$

Marguerre's simultaneous non-linear partial differential equations above cannot be solved exactly; however, several approximate analytical and numerical solving methods exist [53]. In this article, a modification of the methods of Levy [54] and Coan [55] is presented. The original method of Levy assumes an approximated deflection shape for $w(x,y)$ that does not change during deformation (Eqs. (7) and (14)):

$$w_0(x,y)=C_0\sin\left(\frac{m\pi x}{a}\right)\sin\left(\frac{n\pi y}{b}\right) \tag{14}$$

This deflection shape is substituted in compatibility Eq. (13), which once solved, yields a solution for the Airy stress function. This solution consists of the normal non-homogeneous part but also of additional homogeneous solution parts that take into account different boundary conditions for a plate as shown in Fig. 5. The added solutions parts are given by Murray [53] and Levy et al. [56] for the $K1$ and $K2$ parts respectively.

$$\begin{aligned}\Phi=&\frac{E(C^2-C_0{}^2)}{32}\left(\frac{a^2n^2}{b^2m^2}\cos\left(\frac{2m\pi x}{a}\right)+\frac{b^2m^2}{a^2n^2}\cos\left(\frac{2n\pi y}{b}\right)\right)\\&+\frac{1}{2}\sigma_{x;av}y^2+K1\cdot\left(\frac{(C^2-C_0{}^2)n^2\pi^2E}{16b^2}+\frac{\nu\sigma_{x;av}}{2}\right)x^2\\&+K2\cdot E\left(\begin{matrix}T1\cdot\cosh\left(2m\pi\left(\frac{y}{a}-\frac{b}{2a}\right)\right)+\\T2\cdot2m\pi\left(\frac{y}{a}-\frac{b}{2a}\right)\sinh\left(2m\pi\left(\frac{y}{a}-\frac{b}{2a}\right)\right)\end{matrix}\right)\cos\left(\frac{2m\pi x}{a}\right)\end{aligned} \tag{15}$$

$$\begin{aligned}T2=&\frac{a^2n^2(C^2-C_0{}^2)(a/bm\pi)\sinh(bm\pi/a)}{32b^2m^2\left(1+(a/2bm\pi)\sinh(2bm\pi/a)\right)}\quad\wedge\\T1=&-T2\left(1+\frac{bm\pi}{a}\coth\left(\frac{bm\pi}{a}\right)\right)\end{aligned} \tag{16}$$

The Airy stress function Eqs. (15) and (16) and the assumed deflection shape Eqs. (7) and (14) can be substituted in the equilibrium Eq. (12), which then yields a function that relates the average loading stress $\sigma_{x;av}$ and the deflection magnitude C for a given imperfection C_0. However, in this paper, a modification of Levy's method is presented that has the advantage that the stability of the equilibrium state can be monitored during deformation, which is needed in Section 4. It does not use the equilibrium differential Eq. (12), but the principle of minimal potential energy (which yields equilibrium) instead. The potential energy V equals the load potential L_p plus the strain energy that consists of membrane energy (U_m), bending energy (U_b), and energy due to twisting (U_t):

$$\begin{aligned}V=&L_p+U_m+U_b+U_t=-\sigma_{x;av}\,btu_{x;av}\\&+\frac{1}{2}tE\int\int\left(\left(\frac{\partial^2\Phi}{\partial x^2}+\frac{\partial^2\Phi}{\partial y^2}\right)^2-2(1+\nu)\left(\frac{\partial^2\Phi}{\partial x^2}\frac{\partial^2\Phi}{\partial y^2}-\left(\frac{\partial^2\Phi}{\partial x\partial y}\right)^2\right)\right)dxdy\\&+\frac{1}{2}D\int\int\left(\left(\frac{\partial^2\overline{w}}{\partial x^2}+\nu\frac{\partial^2\overline{w}}{\partial y^2}\right)\frac{\partial^2\overline{w}}{\partial x^2}+\left(\frac{\partial^2\overline{w}}{\partial y^2}+\nu\frac{\partial^2\overline{w}}{\partial x^2}\right)\frac{\partial^2\overline{w}}{\partial y^2}\right)dxdy\\&+D\iint(1-\nu)\left(\frac{\partial^2\overline{w}}{\partial x\partial y}\right)^2dxdy\end{aligned} \tag{17}$$

with $u_{x;av}$ being the edge displacement of the loaded edge. Using $\overline{w}=w-w_0$, Eqs. (7) and (14)–(16) can be substituted in Eq. (17). Subsequently, making the potential energy stationary yields the function that relates the average loading stress $\sigma_{x;av}$ and the deflection magnitude C for a given imperfection C_0:

$$\begin{aligned}\sigma_{x;av}=&-\frac{(1-C_0/C)n^2t^2\pi^2E}{48b^2(1-\nu^2)}\left(1-K1\cdot\frac{1}{1+(b^2m^2/a^2n^2\nu)}\right)*\\&\left(\begin{matrix}\left(8+\left(\frac{m^2b^2}{n^2a^2}+\frac{n^2a^2}{m^2b^2}\right)\left(4+3\frac{C^2}{t^2}\left(1+\frac{C_0}{C}\right)(1-\nu^2)\right)\right)+\\6(K1+K2)\frac{n^2a^2}{m^2b^2}\frac{C^2}{t^2}\left(1+\frac{C_0}{C}\right)(1-\nu^2)*\\\left(K1-K2\frac{((a/bm\pi)\sinh(bm\pi/a))^2}{1+(a/2bm\pi)\sinh(2bm\pi/a)}\right)\end{matrix}\right)\end{aligned} \tag{18}$$

Also, using kinematical relationships, and substituting Eqs. (7) and (14)–(16) herein, the average in-plane displacement of the loaded edge can be shown to equal

$$\begin{aligned}u_{x;av}=&\int_0^a\left(\varepsilon_x dx-\frac{1}{2}\left(\frac{\partial w}{\partial x}\right)^2dx+\frac{1}{2}\left(\frac{\partial w_0}{\partial x}\right)^2dx\right)=\\&-\frac{(C^2-C0^2)\pi^2n^2a((b^2m^2/a^2n^2)+K1\nu)}{8b^2}+\frac{a(1-K1\nu^2)\sigma_{x;av}}{E}\end{aligned} \tag{19}$$

Now using formulae (10) and (11) and (18) and (19), the linear stiffness before buckling and after buckling can be determined for plates without an imperfection. This is shown in Fig. 6 with dotted lines for loads up to twice the buckling load, for all 3 possible boundary conditions. Also, using the same formulae, the nonlinear elastic behaviour can be determined for plates with an

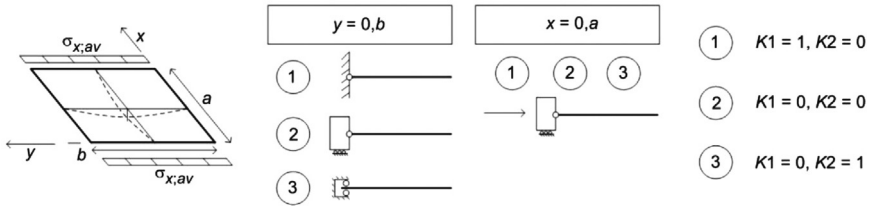

Fig. 5. *K*1 and *K*2 values (as used in Eqs. (15) and (16)) for plate with different sets (1–3) for the boundary conditions.

imperfection (arbitrarily chosen to be equal to the plate thickness) and this behaviour is shown with a continuous line, also for all three possible boundary conditions.

It is interesting to note that for $K1=0$ and $K2=1$ (see Fig. 5), Rhodes obtained a prediction for the post/pre-buckling stiffness ratio by curve fitting of numerical results [57]. However, now using Eqs. (10), (18) and (19), and Mathematica [58], it is possible to find an exact solution as follows:

$$\frac{E_{post}}{E_{pre}} = \frac{a(\sigma_{x;av}-\sigma_{x;cr})/(u_{x;av}-u_{x;cr})}{E} = \frac{((b/a)^4+1)(1+(a/2b\pi)\sinh(2b\pi/a))-2(a/b\pi)^2\sinh(b\pi/a)^2}{(3(b/a)^4+1)(1+(a/2b\pi)\sinh(2b\pi/a))-2(a/b\pi)^2\sinh(b\pi/a)^2} \tag{20}$$

The exact solution above can be used to prove that Rhodes expectation is correct that values obtained with his curve-fitting approach are close enough to the exact values for the range $0.4<a/b<4$. This "close enough" is now quantified to be a maximal error of 1.45%.

3.2. Elastic, far post-buckling behaviour

The approximate method to describe the post-buckling behaviour, as explained in the previous section, yields only reliable results for loads up to about twice the buckling load. For loads larger than about twice the buckling load, the buckling shape is no longer the same as the initial buckling shape, actually changes continuously, and this change needs to be accounted for. For this, the deflection shape is described by a double Fourier series, as introduced by Levy [54]:

$$w(x,y) = \sum_{m=1,2,\ldots}^{\infty}\sum_{n=1,2,\ldots}^{\infty} w_{m,n}\sin\left(m\frac{\pi x}{a}\right)\sin\left(n\frac{\pi y}{b}\right)$$
$$w_0(x,y) = \sum_{m=1,2,\ldots}^{\infty}\sum_{n=1,2,\ldots}^{\infty} w_{0m,n}\sin\left(m\frac{\pi x}{a}\right)\sin\left(n\frac{\pi y}{b}\right) \tag{21}$$

Now, the same strategy is followed as used in Section 3.1. The deflection shape of Eq. (21) is again substituted in compatibility Eq. (13), which once solved, yields as a solution the homogeneous part of the Airy stress function. Additional to this part, homogeneous solution parts are included that take into account the different boundary conditions for a plate as shown in Fig. 5. These additional parts are derived in [59] and based on the work of Murray [53] and Levy et al. [54]:

$$\Phi = \sum_{p=0,1,2,\ldots}^{\infty}\sum_{q=0,1,2,\ldots}^{\infty}(b_{p,q}-b_{0p,q})\cos\left(p\frac{\pi x}{a}\right)\cos\left(q\frac{\pi y}{b}\right)+\frac{1}{2}\sigma_{x;av}y^2$$
$$+K1*\left(\sum_{m=1,2,\ldots}^{\infty}\sum_{n=1,2,\ldots}^{\infty}\frac{(w_{m,n}^2-w_{0m,n}^2)n^2\pi^2E}{16b^2}+\frac{\nu\sigma_{x;av}}{2}\right)x^2$$
$$+K2\cdot\left(\begin{array}{l}\sum_{p=2,4,\ldots}^{\infty}\left(C1\cosh\left(\frac{p\pi b}{2a}\left(\frac{2y}{b}-1\right)\right)+C2\,\frac{p\pi b}{2a}\left(\frac{2y}{b}-1\right)\sinh\left(\frac{p\pi b}{2a}\left(\frac{2y}{b}-1\right)\right)\right)+\\ \sum_{p=1,3,\ldots}^{\infty}\left(C3\sinh\left(\frac{p\pi b}{2a}\left(\frac{2y}{b}-1\right)\right)+C4\,\frac{p\pi b}{2a}\left(\frac{2y}{b}-1\right)\cosh\left(\frac{p\pi b}{2a}\left(\frac{2y}{b}-1\right)\right)\right)\end{array}\right)$$

$$\text{with } b_{p,q} = \frac{E}{4(p^2b/a+q^2a/b)^2}(B_1+B_2+B_3+B_4+B_5+B_6+B_7+B_8+B_9) \tag{22}$$

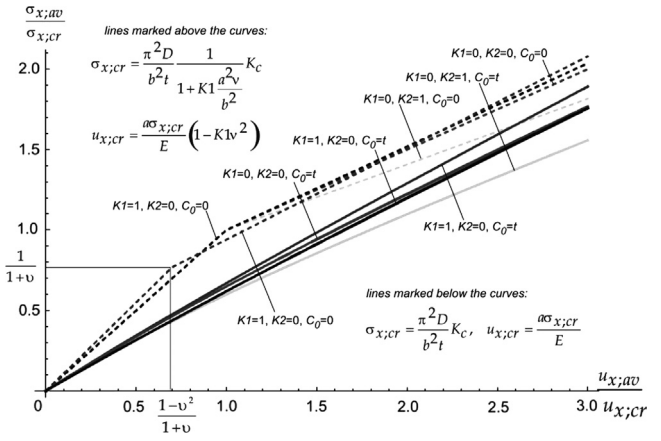

Fig. 6. Load (stress) vs. displacement curves for plates with and without imperfections; see Fig. 5 for the meaning of the *K*1 and *K*2 values.

Terms B_i are given in [54], and if the deflection shape is truncated with m_{max} and n_{max}, then the stress function is truncated at $p_{max}=m_{max}$ and $q_{max}=n_{max}$. Factors C1–C4 equal

$$C1 = -C2\left(1+\frac{bp\pi}{2a}\coth\left(\frac{bp\pi}{2a}\right)\right)$$
$$C2 = \frac{(2a/bp\pi)\sinh(bp\pi/2a)}{(1+(a/bp\pi)\sinh(bp\pi/a))}\sum_{q=0,1,2,\ldots}^{\infty}(b_{p,q}-b_{0p,q})$$
$$C3 = -C4\left(1+\frac{bp\pi}{2a}\tanh\left(\frac{bp\pi}{2a}\right)\right)$$
$$C4 = \frac{(2a/bp\pi)\cosh(bp\pi/2a)}{(1-(a/bp\pi)\sinh(bp\pi/a))}\sum_{q=0,1,2,\ldots}^{\infty}(b_{p,q}-b_{0p,q}) \tag{23}$$

The displacement functions and stress function (Eqs. (21)–(23)) are substituted in the potential energy formulation (Eq. (17)), whereafter the potential energy is obtained by integrating twice. However, regular integration of the potential energy is shown to be very time-consuming in Mathematica, such that not more than 3 coefficients can be used. For a (truncated) double sine Fourier series as displacement function, and boundary conditions for which $K2=0$, a special procedure has been developed in Mathematica, yielding a 16 times more efficient procedure than the regular and single command. This procedure is shown in Fig. 7.

Once the potential energy is found, it should be made stationary. This yields m_{max} times n_{max} equations, each containing an equal number of deflection coefficients and $\sigma_{x;av}$. These equations cannot be solved exactly and thus are treated numerically (using the NSolve command in Mathematica). A major disadvantage of this strategy is that no direct formula can be derived between the average stress $\sigma_{x;av}$ and the deflection coefficients. Note that solving the equations may result in more than one combination of coefficients satisfying equilibrium, i.e. representing several equilibrium states.

Naturally, adding more terms to the deflection shape results in a more accurate description of the post-buckling behaviour, however, also in a longer computation time. The effect of utilising more coefficients on the post-buckling behaviour for a square

$$\int_0^b \int_0^a \text{expression}\, dx\, dy$$

'Standard' *Mathematica* integration:

```
Integrate[expression, {x, 0, a}, {y, 0, b}]
```

Integration rule:

```
integreer[integreer[expression, {x, a}], {y, b}]
```

```
integreer[expr_, {xy_, ab_}] :=
 Block[{ca, csx, inta, A, aa},
  csx = Union[Extract[expr, Position[expr, Cos[___ * (xy / ab)] | Sin[___ * (xy / ab)]]]];
  If[csx == {}, ab * expr, ca = CoefficientArrays[expr, csx];
   ca[[1]] * ab + If[Length[ca] > 1, ca[[2]].Integrate[csx, {xy, 0, ab}] +
       If[Length[ca] > 2, A = Array[aa, {Length[csx], Length[csx]}];
        Integrate[A.csx.csx, {xy, 0, ab}] /. Thread[Flatten[A] → Flatten[Normal[ca[[3]]]]], 0], 0]]
```

Fig. 7. Mathematica integration rule to make integration of potential energy more efficient.

plate with fixed unloaded edges ($K1=0$, $K2=0$) is shown in Fig. 8, which for now only shows stable equilibrium paths. For the far post-buckling behaviour branches, the deflection shape is primarily determined by the initial post-buckling term, $w_{1.1}$. The subscripts of w refer to m and n values of Eq. (21). If the average stress is increased from the critical stress, the magnitudes of the other terms ($w_{1.3}$, $w_{3.1}$ and $w_{3.3}$) start to increase in relation to the magnitude of $w_{1.1}$. This corresponds to the previous statement that after buckling the deflection shape slowly alters from the initial deflection shape. Besides the far-post buckling behaviour for several deflection coefficients combinations, a solution by Williams and Walker is added, including a list of their coefficients A and B [60]. The coefficients (A and B) of their solution yield results that are only suitable for a load up to twice the buckling load.

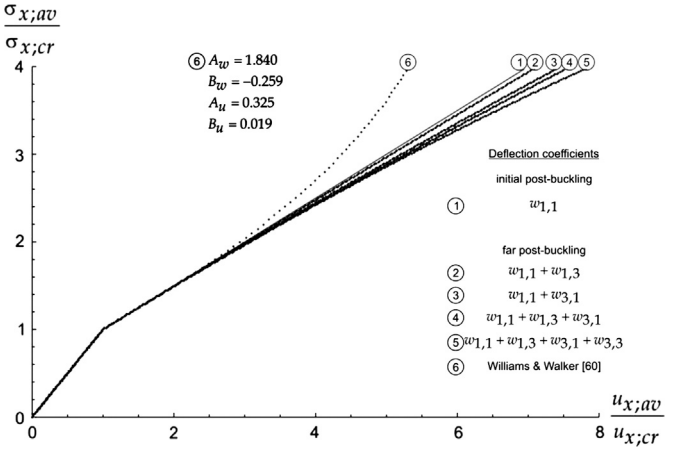

Fig. 8. Second order post-buckling behaviour in comparison with first order ($a=b$, $K1=0$ and $K2=0$).

4. Mode jumping

Mode jumping was first observed in experiments presented by Stein [61]. He noticed changes in the number of buckles (from 5 to 6 to 7 etc.) for a stiffened panel under compression, and these changes occurred in a violent way. And much later, Riks et al. presented conclusions of several mode jumping studies and developed a fundamental framework for solving mode jumping phenomena by the finite element method [62].

For thin-walled trapezoidal sheeting, mostly having a long flange under compression, Hofmeyer and Jaspart, for several reasons, suspected mode jumping to possibly occur [51]. This in turn could cause the developed design rules to be invalid, or at least subject to serious reconsiderations. Therefore, a theoretical understanding and description of mode-jumping behaviour was required, which is now condensed in this article.

4.1. Analytical description

In the previous section, the first variation of the potential energy was used to determine the equilibrium state. It can then be understood easily that the second variation (involving second derivatives of the potential energy) yields information on the stability of this equilibrium. Namely, if the second variation is positive for all possible variations, the potential energy is locally increasing everywhere and thus a minimum of potential energy exists, which is equivalent to a stable equilibrium. Likewise, a positive second variation is equivalent with an unstable equilibrium. If the second variation would be zero, it would indicate critical stability. For determining the far post-buckling behaviour, deflections coefficients $w_{i,j}$ were used, and as such

$$\delta^2 Epot = \sum_{i,j,k,l=1}^{m,n,m,n} \frac{\partial^2 Epot}{\partial w_{i,j} \partial w_{k,l}} \delta w_{i,j} \delta w_{k,l} \triangleq \boldsymbol{\delta w}^{\mathbf{T}} \mathbf{A} \boldsymbol{\delta w} > 0 \tag{24}$$

Thus, the equilibrium state is stable if matrix **A** is positive definite, which is the case if all diagonal terms are positive and the determinant of **A** is positive as well. Using the same approach as in the previous section, stability was determined for the square plate in Fig. 8 (for shape function group "5": $w_{1,1}+w_{1,3}+w_{3,1}+w_{3,3}$) and results are shown in Fig. 9: from the branch that represents the state of a flat remaining plate (which is the linear branch starting in the origin and ending at (10,10)), three branches originate, corresponding *initially and by definition* to the first (stable), second (unstable), and third (unstable) buckling mode. But note that for ongoing deformations, the coefficients values will change and every curve represents a superposition of several deformations modes. Normally, it is expected that the plate will follow the stable first buckling mode branch. Hereafter, at a load of four times the (first) buckling load, several stable and unstable branches intersect. Again, one expects the plate will remain in the first buckling mode branch, because the branch is stable and the deformation shape of the other (intersecting) stable branch differs. At a load of around eight times the (first) buckling load, the first buckling mode branch terminates. This means that when the load is increased from that point on, no (static) equilibrium exists and the plate will probably move towards another stable branch (i.e. here the branch belonging to the second buckling mode). The connecting path from the original stable branch to the new stable

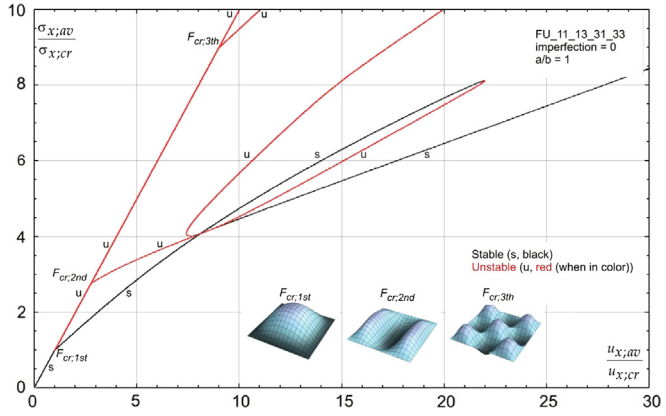

Fig. 9. Analytically determined stability of second order post-buckling behaviour ($a=b$, $K1=0$ and $K2=0$).

branch is associated with mode-jumping, but cannot be obtained here, because it follows the differential equations for dynamic behaviour (e.g. via d'Alembert's principle), which are not used here.

Furthermore, it is possible that the limited number of deflection coefficients used may hide other possible stable or unstable branches, and may also terminate the first buckling mode curve undeserved. To investigate these issues, more deformation coefficients should be taken into account; however, this is much too time consuming using the "NSolve" approach in Mathematica. Another approach is possible (using the "FindRoot" command), but here only a single solution is found for a certain load, and starting values for the (varying) coefficients have to be varied randomly to obtain more solutions (i.e. branches). In this way, no guarantees can be given anymore that all existing branches are found. As an example, using this approach, for the plate in Fig. 9 several additional coefficients were taken into account (w_{11}, w_{13}, w_{15}, w_{31}, w_{33}, w_{35}, w_{51}, w_{53}, w_{55}). This resulted in discovering one additional buckling mode spring-off branch with no further consequences on the predicted overall behaviour.

Note also that the type of behaviour above is quite similar to the behaviour obtained by Stein for an elastic column supported by springs [63] and other similar spring structures [64].

4.2. Finite element simulations

The Mathematica integration rule in Fig. 7, used with the analytical description above, has only be used for in-plane boundary conditions $K1=0$ and $K2=0$. It is expected to be also applicable for $K1=1$ and $K2=0$, but not for $K1=0$ and $K2=1$ as these boundary conditions introduce hyperbolic sine and hyperbolic cosine functions in the Airy stress function. In this section, a finite element model is developed (1) to verify the analytical description for plates with straight remaining unloaded edges and (2) to be able to study plates with unloaded edges free to wave in-plane ($K1=0$ and $K2=1$).

The finite element approach to obtain the post-buckling behaviour above consists of two parts. First an eigen-mode analysis is carried out and the results are saved. Next, this analysis is followed by either an implicit transient analysis or an explicit transient analysis. For the implicit and explicit transient analysis parts, separate models are used because they are carried out by different environments in the FE program used, ANSYS Mechanical APDL 12.0.1 [65].

4.2.1. Eigen-mode analysis

The model used for determining the eigen-modes is shown in Fig. 10. All edges of the model are simply supported and are loaded by a displacement in x-direction of the edge at $x=+/-\ a/2$ (thus the stress and strain in the plate are constant). In y-direction $NE1$ elements are applied and in x-direction $NE1\times a/b$ elements, which will result in square elements for every value of a/b (as long as a/b yields an integer). The element used to mesh the plate is a four-node shell element, "SHELL181". First, the calculation of the eigen-modes starts with performing a static analysis with pre-stress effects. Next, a buckling analysis is performed using the subspace solution method and the first three eigen-modes are extracted. The eigen-modes are saved and will be used in the next (explicit and implicit) analyses as shape for the initial imperfection.

4.2.2. Explicit analysis

Regarding the set-up, for the explicit analysis as shown in Fig. 11, two types of imperfection have been used: BS, which means a single or a combination of eigen-modes as found with the analysis above, or M, which is an imperfection by assuming a sinusoidal deflection shape (the number of sine waves in x-direction to be selected). Secondly, analyses have been carried out as defined by abbreviation E, linear material behaviour, and EP, being nonlinear material behaviour, which introduces yielding of the material. Finally, different boundary conditions have been used for the unloaded edges, abbreviated by the factors $K1$ and $K2$ as shown in Figs. 5 and 11.

With respect to loading, the in-plane full displacement of the loaded edges is performed at 150 ms, which is much faster than normal quasi-static experiments. For this, research on simply supported square plates revealed that a small value of alpha damping (1000), applied to all elements, is useful for damping out oscillations in the reaction forces without compromising the static behaviour of the structure significantly [66]. Use of damping may also be a necessity as Riks states "It is finally noted that the damping is taken into account to serve two properties: to let the simulation be as close as possible to the actual behaviour of the structure and to make sure that convergence to a new stable state after a jump will actually take place" [62]. The prescribed velocity function is linearly increasing, resulting in a quadratic displacement function. It was found that linear increasing velocities are better suited for loading changing structure shapes, due to the slow displacement in the first part of the loading function [66].

For the material, an isotropic elastic material model was used, with density $\rho=7.83\text{E}-006$ kg/mm^3, Young's modulus $E=210{,}000$ N/mm^2, and $\upsilon=0.3$. Four node shell elements "SHELL163" were used, with a Belytschko–Tsay formulation. For the number of integration points along the element height, 3 was chosen, to enable reasonable plastic behaviour in bending. The plasticity behaviour was described with the so-called PLAW model (piecewise linear plastic model for explicit element only) [65].

4.2.3. Implicit analysis

In this research, the implicit analysis model is almost the same as the explicit model except (1) SHELL 181 [65] is used, because SHELL163 [65] is not applicable for implicit analyses, and (2) for

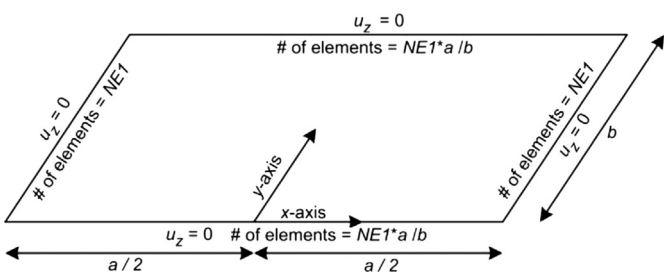

Fig. 10. Finite element model for eigen-mode analyses; NE1 stands for Number of Elements variable 1.

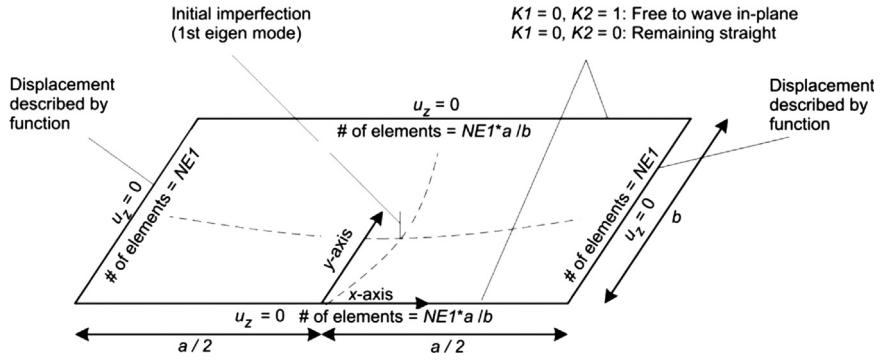

Fig. 11. Finite element model for explicit analyses; NE1 stands for Number of Elements variable 1.

the same reason, material behaviour is described by the so-called BISO model (bilinear kinematic hardening using von Mises or Hill plasticity [65]).

4.2.4. Square plate results

To validate the analytical approximation method as presented in Section 4.1, FE simulations of a square plate have been performed, as shown in Fig. 12. All FE simulations here use a manually defined imperfection (M) to ensure exact similar initial imperfections. The results from the analytical approximation method have been obtained without an imperfection, but the difference is negligible because the assumed imperfection in the FE analyses is extremely small compared to the plate's thickness. Branches 1 and 2 in Fig. 12 present the initial post-buckling behaviour of a plate with the unloaded edges respectively remaining straight and free to wave in-plane, according to Section 3.1. Branches 2 and 3 present explicit FE simulation results of the plate, again with the unloaded edges respectively remaining straight and free to wave in-plane. Branch 5 is equal to branch 3, although now generated by an implicit analysis as presented in Section 4.2.3. Branches 6 and 7 represent the behaviour obtained by the analytical approximation method (with FindRoot, Section 4.1). While branch 6 is dominated by $w_{1,1}$, branch 7 is dominated by the deflection coefficient $w_{3,1}$. Branch 8 is equal to branch 4, although now bilinear elasto-plastic material behaviour is assumed.

It can be seen that branch 3, for unloaded edges to remain straight, shows a mode-jumping phenomenon at $u_{av}/u_{cr}=20.5$. The corresponding load is $\sigma_{av}=7.266\,\sigma_{cr}$. The deflection shape of the plate before and after the mode jump has been presented in Fig. 13. If the unloaded edges are not restricted to remain straight, no mode-jumping occurs, curve 4.

The implicit equivalent of branch 3, branch 5, shows exactly the same results and the implicit mode-jump load ($\sigma_{av;modejump,exp}=7.296\,\sigma_{cr}$) only slightly differs from the former explicit simulation. For both simulations, after buckling and after mode-jumping the branches show oscillations which represent vibrations (oscillations) around the new stable path.

The curves of the analytical approximation method (curves 6 and 7) are completely coinciding with the simulations, but – of course – do not incorporate the dynamic transition between the two buckling modes. Small differences may be caused by the fast loading time and damping used in the simulations.

Finally, it can also be observed that if elasto-plastic material behaviour is used (curve 8), for this case no mode-jumping occurs. However, this is certainly not a general applicable conclusion.

4.2.5. Long plate results

Stein states that, "… preliminary calculations have indicated that for length–width ratios near unity the change in buckle pattern would be rather abrupt; whereas for higher length–width ratios changes in buckle pattern would be continuous or, at least, would be less abrupt." [61]. Therefore, in this section the behaviour of long plates will be discussed. For this, three additional analyses have been carried out, equal to the simulation of curve [3] in Fig. 10, but now different for their length/width ratios: $a/b=5$, $a/b=10$, and $a/b=14$. Fig. 14 shows the $a/b=10$ simulation, being typical for the other simulations as well. The simulations show mode-jumping always occurring due to one or multiple sets of a single half sine wave splitting up into three half sine waves, in the same way as observed for the square plate in Fig. 13. As such, the number of half sine waves will always increase with 2 (in case of one set), 4 (in case of two sets) or 6, and so on, half sine waves in the compressed direction. The reason why sometimes only one splitting set occurs and other times multiple sets (at the same time) is unknown. But a reason may be that for a long plate the different stress-shortening curves (thus for a different number of half sine waves) are positioned closer to each other than for a short plate.

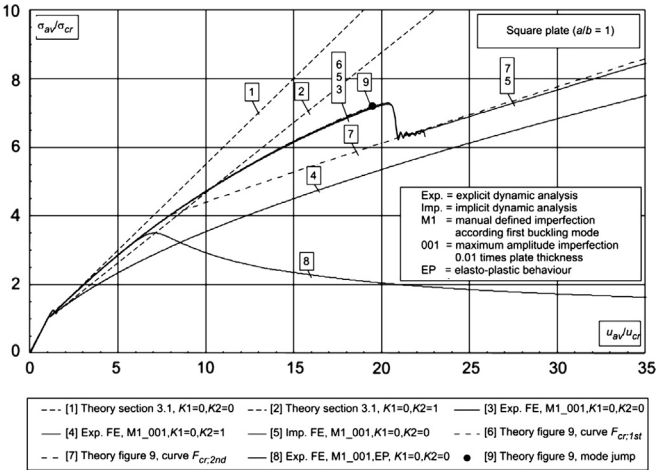

Fig. 12. Results for FE simulations of a square plate.

5. Conclusions

A recently developed model to predict the failure behaviour of trapezoidal sheeting left the question open whether mode jumping (the phenomenon that a plate dynamically changes its buckling mode during an increasing load) should be taken into account in the model. To answer this question, in this article a study on the phenomenon of mode-jumping was presented. Mode-jumping was investigated by using two methods. First, it was analysed by the analytical approximation method that has been introduced in Section 4.1. A spin-off of the analytical model is a new and

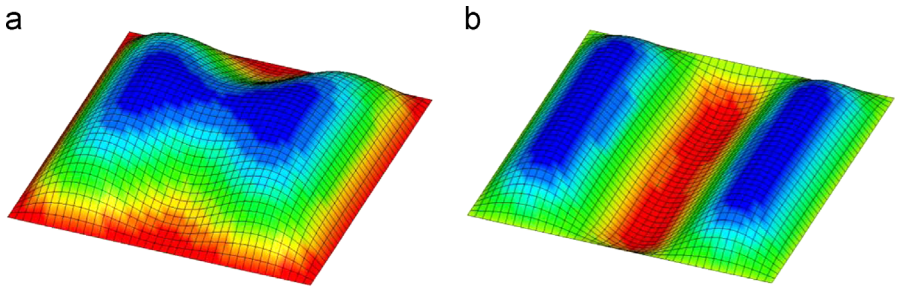

Fig. 13. Scaled deflections shape of curve [3] of Fig. 11 (a) before and (b) after mode-jumping.

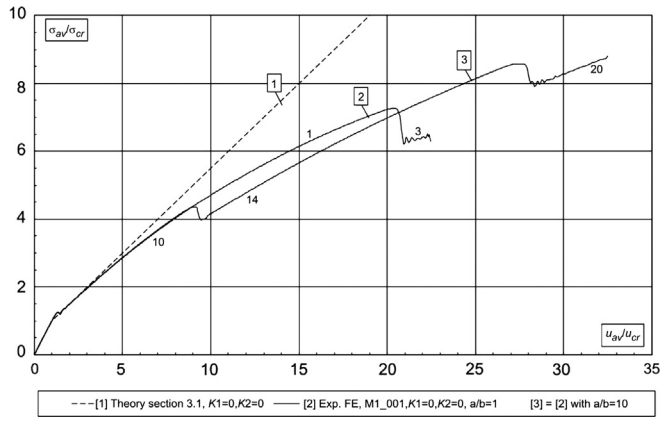

Fig. 14. Results for a long plate ($a/b=10$) vs. a square plate ($a/b=1$).

analytical expression for a currently curve-fitted prediction formula for the post/pre-buckling stiffness ratio by Rhodes. Furthermore, it was shown that the accuracy range of a solution by Williams and Walker for the far-post buckling behaviour can be confirmed. Secondly, mode-jumping was analysed using the finite element method (explicit and implicit dynamic), as presented in Section 4.2.

Related to qualitative behaviour, both methods indicate that mode-jumping occurs by a single (or more) half sine wave that splits into three half sine waves. Therefore, after mode-jumping, the number of half sine waves are predicted to increase with a multiple of two half sine waves (in the compressed direction). However, this does not correspond to experimental findings by Stein [61]. His experiments showed that when mode-jumping occurs, the number of half sine waves increases with a single wave and the deflection shape changes consecutively from symmetrical to asymmetrical (in compressed direction). The reason for this discrepancy could be the existence of more serious imperfections in practice (most likely) or – related to this – boundary conditions for the experiments that are not perfectly documented and thus cannot be replicated. After all, the models in this article describe a perfect situation, except for the quite subtle imperfections applied deliberately to initiate mode-jumping.

Related to quantitative behaviour, it was shown that the prediction of the load at which mode-jumping is initiated by both methods corresponds extremely well. The prediction can be improved for the analytical approximation method by adding more deflection coefficients, which results in a more accurate deflection shape. For the finite element analyses it is shown that more elements yield a more accurate prediction of the mode-jumping load.

Based on the finite element analyses, it can be concluded that for plates with longitudinal unloaded edges that are free to wave-in, mode-jumping does not occur. Thus, it is highly unlikely that the phenomenon occurs in the compressed flange of trapezoidal sheeting that is subjected to a combination of a concentrated load and a bending moment. This because the unloaded edges of the compressed flanges are barely supported inwards by the webs.

The analytical approximation method results are so promising that the method could possibly be extended along with the finite element model to solve the previous mentioned discrepancy between these methods and experimental observations. An advantage of the analytical approximation method over finite element simulations is that it finds all the equilibrium paths (stable as well as unstable) which might yield more information for solving the discrepancy. A disadvantage of the analytical method is that no transition paths can be found because these paths do not represent a static equilibrium state. Future research could, besides finite element simulations for full sheeting [67], also involve (a) the determination of mode jumping behaviour of plates with stiffeners, (b) the failure behaviour of plates with stiffeners, and (c) experiments to further verify the analytical and finite element models presented in this paper.

Acknowledgements

M.Sc.-student J. Courage carried out the research as presented in this article. His work was rewarded by the Dutch national first prize “StudentenSTAALprijs 2011”. Besides by the first author, he was supervised by Full Professor Dr. J.G.M. Kerstens and Full Professor F. Soetens, both from within the group. Their help is appreciated as well. W.J.P.M. Kortsmit, M.Sc., a colleague from our University’s Department of Mathematics and Computer Science, developed a more efficient Mathematica procedure that enables the integration of potential energy for a relevant number of coefficients. His help is highly acknowledged.

References

[1] Macdonald M, Heiyantuduwa MA, Rhodes J. Finite element analysis of web crippling behaviour of cold-formed steel flexural members. In: Proceedings of the 18th international specialty conference on cold-formed steel structures: recent research and developments in cold-formed steel design and construction. Orlando, FL; 2006.

[2] MacDonald M, Heiyantuduwa MA. A design rule for web crippling of cold-formed steel lipped channel beams based on nonlinear FEA. Thin-Walled Structures 2012;53:123–30.

[3] MacDonald M, Heiyantuduwa Don MA, Kotełko M, Rhodes J. Web crippling behaviour of thin-walled lipped channel beams. Thin-Walled Structures 2011;49(5):682–90.

[4] Tse WT, Chung KF. Web crippling behaviour of laterally restrained cold-formed steel re-entrant profiled deckings. Journal of Constructional Steel Research 2008;64(7–8):785–801.

[5] Zhou F, Young B. Experimental and numerical investigations of cold-formed stainless steel tubular sections subjected to concentrated bearing load. Journal of Constructional Steel Research 2007;63(11):1452–66.

[6] Akhand AM, Wan Badaruzzaman WH, Wright HD. Combined flexure and web crippling strength of a low-ductility high strength steel decking: experiment and a finite element model. Thin-Walled Structures 2004;42(7):1067–82.

[7] Biegus A, Czepiżak D. Research on the interactive resistance of corrugated sheets under combined bending and contact pressure. Thin-Walled Structures 2006;44(8):825–31.
[8] Biegus A, Czepizak D. Experimental investigations on combined resistance of corrugated sheets with strengthened cross-sections under bending and concentrated load. Thin-Walled Structures 2008;46(3):303–9.
[9] Chen DH. The collapse mechanism of corrugated cross section beams subjected to three-point bending. Thin-Walled Structures 2012;51:82–6.
[10] Guzelbey IH, Cevik A, Erklig A. Prediction of web crippling strength of cold-formed steel sheetings using neural networks. Journal of Constructional Steel Research 2006;62(10):962–73.
[11] Hedaoo NA, Gupta LM, Ronghe GN, Parikh SK. State of the art report on thin-walled cold-formed profiled steel decking. In: Proceedings of the 19th international specialty conference on recent research and developments in Cold-formed steel design and construction. MO: St. Louis; 2008. p. 307–23.
[12] Langdon GS, Schleyer GK. Deformation and failure of profiled stainless steel blast wall panels. Part III: Finite element simulations and overall summary. International Journal of Impact Engineering 2006;32(6):988–1012.
[13] European standard EN 1993-1-3:2006(E). Eurocode 3-design of steel structures—Part 1–3: general rules–supplementary rules for cold-formed members and sheeting. European committee for standardization, Rue de Stassart 26, B-1050 Brussels.
[14] North American specification for the design of cold-formed steel structural members, 2007 edition, and commentary on specification, 2007 edition. American Iron and Steel Institute, 1140 Connecticut Ave., NW, Suite 705 Washington, D.C, 20036, USA.
[15] Von Kármán T, Sechler EE, Donnel LH. The strength of thin plates in compression. Transactions of the American society of mechanical engineers APM-54-5; 1931.
[16] Winter G. Strength of thin steel compression flanges, with appendix. Bulletin 35/3. Ithaca, NY: Cornell University Engineering Experiment Station; 1947.
[17] Schafer BW. Review: the direct strength method of cold-formed steel member design. In: Proceedings of SDSS2006, international colloquium on stability and ductility of steel structures. Lisbon, Portugal: IST Press; September 06–082006. isbn:978-972-8469-61-06.
[18] Rusch A, Lindner J. Remarks to the direct strength method. Thin-Walled Structures 2001;39(9):807–20.
[19] Winter G, Pian RHJ. Crushing strength of thin steel webs. Cornell Bulletin 1946;35(pt. 1).
[20] Zetlin L. Elastic instability of flat plates subjected to partial edge loads. Journal of the Structural Division ASCE 1955:81.
[21] Hetrakul N, Yu WW. Structural behaviour of beam webs subjected to web crippling and a combination of web crippling and bending. Final report. Civil engineering study 78-4. Rolla, MO: University of Missouri-Rolla; June 1978.
[22] Yu WW. Web crippling and combined web crippling and bending of steel decks. Civil engineering study 81-2. Rolla, MO: University of Missouri-Rolla; April 1981.
[23] Santraputra C. Web crippling of high strength cold-formed steel beams [Ph.D. thesis]. Rolla, MO: University of Missouri-Rolla; 1986.
[24] Santraputra C, Parks MB, Yu WW. Web crippling strength of cold-formed steel beams. Journal of Structural Engineering 1989;115:10.
[25] Bhakta BH, LaBoube RA, Yu WW. The effect of flange restraint on web crippling strength. Civil engineering study 92-1. Rolla, MO: University of Missouri-Rolla; March 1992.
[26] Langan JE, LaBoube A, Yu WW. Structural behaviour of perforated web elements of cold-formed steel flexural members subjected to web crippling and a combination of web crippling and bending. Civil engineering series 94-3. Cold-formed steel series. Department of Civil Engineering. Rolla, MO: University of Missouri-Rolla; 1994.
[27] Cain DE, LaBoube RA, Yu WW. The effect of flange restraint on web crippling strength of cold-formed steel Z- and I-sections. Civil engineering study 95-2. Rolla, MO: University of Missouri-Rolla; May 1995.
[28] Wu S, Yu WW, LaBoube RA. Strength of flexural members using structural grade 80 of A653 steel (web crippling tests). Third Progress Report. Civil engineering study 97-3. Rolla, MO: University of Missouri-Rolla; February 1997.
[29] Wing BA. Web crippling and the interaction of bending and web crippling of unreinforced multi-web cold-formed steel sections (M.A.Sc. thesis). Waterloo, Canada: University of Waterloo; 1981.
[30] Wing BA, Schuster RM. Web crippling of decks subjected to two-flange loading. In: Proceedings of the sixth international speciality conference on cold-formed steel structures. Rolla, MO: University of Missouri-Rolla; November 1982.
[31] Prabakaran K. Web crippling of cold-formed steel sections (M.S. thesis)., Waterloo, Canada: University of Waterloo; 1993.
[32] Gerges RR. Web crippling of single web cold-formed steel members subjected to end one-flange loading (M.A.Sc. thesis). Waterloo, Canada: University of Waterloo; 1997.
[33] Gerges RR, Schuster RM. Web crippling of members using high-strength steels. In: Proceedings of the fourteenth international specialty conference on cold-formed steel structures. Rolla, MO: University of Missouri-Rolla; October 1998.
[34] Prabakaran K, Schuster RM. Web crippling of cold-formed steel members. In: Proceedings of the fourteenth international specialty conference on cold-formed steel structures. Rolla, MO: University of Missouri-Rolla; October 1998.
[35] Beshara B. Web crippling of cold-formed steel members (M.A.Sc. thesis), University of Waterloo, Waterloo, Canada; 1999.
[36] Beshara B, Schuster RM. Web crippling data and calibrations of cold-formed steel members. Final report. Waterloo, Canada: University of Waterloo; 2000.
[37] Beshara B, Schuster RM. Web crippling of cold formed C- and Z-sections. In: Proceedings of the fifteenth international specialty conference on cold-formed steel structures. Rolla, MO: University of Missouri-Rolla; October 2000.
[38] Young B, Hancock GJ. Web crippling behaviour of cold-formed unlipped channels. In: Proceedings of the fourteenth international specialty conference on cold-formed steel structures. Rolla, MO: University of Missouri-Rolla; October 1998.
[39] Hetrakul N, Yu WW. Cold-formed steel I-beams subjected to combined bending and web-crippling. In: Rhodes J, Walker AC, editors. Thin-walled structures-recent technical advances and trends in design, research and construction. London: Granada Publishing Limited; 1980.
[40] Yu WW. Web crippling and combined web crippling and bending of steel decks. Civil engineering study 81-2. Rolla, MO: University of Missouri-Rolla; April 1981.
[41] Yu WW. Cold-formed steel design. 3rd ed. New York, NY: John Wiley & Sons; 2000.
[42] Young B, Hancock GJ. Experimental investigation of cold-formed channels subjected to combined bending and web crippling. In: Proceedings of the fifteenth International specialty conference on cold-formed steel structures. Rolla, MO: University of Missouri-Rolla; October 2000.
[43] Hofmeyer H, Kerstens JGM, Snijder HH, Bakker MCM. New prediction model for failure of steel sheeting subject to concentrated load (web crippling and bending moment). Thin-Walled Structures 2001;39(9):773–96.
[44] Marguerre K. Theorie der gekrümmter plate grosser Formänderdung. In: Proceedings of the fifth international congress applied Mechanics; 1938. p. 38.
[45] Hofmeyer H, Rosmanit M, Bakker MCM. Prediction of sheeting failure by an ultimate failure model using the fictitious strain method. Thin-Walled Structures 2009;47(2):151–62.
[46] Bedair O. Stability of web plates in W-shape columns accounting for flange/web interaction. Thin-Walled Structures 2009;47(6–7):768–75.
[47] Bedair O. Stability analysis of plates with partial restraints using unconstrained optimization techniques. International Journal of Structural Stability and Dynamics 2010;10(3):571–87.
[48] Bedair O. Graphical representation for stability limit state design of wide flange beam-column I-sections. Recent Patents on Engineering 2011;5(3):190–5.
[49] Debowski D, Magnucki K, Malinowski M. Dynamic stability of a metal foam rectangular plate. Steel and Composite Structures 2010;10(2):151–68.
[50] Thanga T, Halabiah B, Sivakumaran KS. Strength of plates of rectangular industrial ducts. Procedia Engineering 2011;14:622–9.
[51] Hofmeyer H, Jaspart JP. On the modelling of compressed long plates related to sheet-section behaviour. In: Mahendran M editor. Proceedings of the fifth international conference on thin-walled structures. Brisbane, Australia: Queensland University of Technology; 2008.
[52] Timoshenko SP, Gere JM. Theory of elastic stability. 2nd ed.McGraw-Hill Kogakusha; 1961.
[53] Murray NW. Introduction to the theory of thin-walled structures. Oxford, England: Clarendon Press; 1984.
[54] Levy S. Bending of rectangular plates with large deflections. National Advisory Committee for Aeronautics report No. 737; 1942. p. 139–57.
[55] Coan JM. Large-deflection theory for plates with small initial curvatures loaded in edge compression. ASME Journal of Applied Mechanics 1951;18(2):143–51.
[56] Levy S, Fienup KL, Woolley RM. Analysis of square shear web above buckling load. National Advisory Committee for Aeronautics. Technical note No. 962; 1945.
[57] Rhodes J. Effective widths in plate buckling. In: Rhodes J, Walker AC, editors. Developments in thin-walled structures, vol. 1. England: Applied Science Publishers; 1982.
[58] Mathematica 8. Wolfram Research, Inc. 100 Trade Center Drive. Champaign, IL 61820-7237, USA.
[59] Courage J., Failure mechanisms of thin-walled trapezoidal steel sheeting. M.Sc. report: research report and appendices. Eindhoven University of Technology. Department of the Built Environment. Structural Design Group; 2011.
[60] Williams DG, Walker AC. Explicit solutions for the design of initially deformed plates subjected to compression. In: Proceedings of the Institute of Civil Engineers; 1975. pp 763–87.
[61] Stein M. Loads and deformations of buckled rectangular plates. NASA technical report R-40. National Aeronautics and Space Administration; 1959.
[62] Riks E, Rankin CC, Brogan FA. On the solution of mode jumping phenomena in thin-walled shell structures. Computer Methods in Applied Mechanics and Engineering 1996;136:59–92.
[63] Stein M. The phenomenon of change in buckle pattern in elastic structures. NASA technical report R-39. National Aeronautics and Space Administration; 1959.
[64] De Kleine D, Hofmeyer H, Bakker MCM. Rigid-link and FE models for first-generation sheet-section failure. Thin-Walled Structures0263-8231 2006;44(12):1240–9.
[65] ANSYS Mechanical APDL 12.0.1. ANSYS, Inc., Southpointe. 275 Technology Drive, Canonsburg, PA 15317, United States of America.
[66] Courage J. Explicit dynamic quasi-static simulations of simply supported square plates (in Dutch). Research report O-2008.3. Structural design group.

Department of the Built Environment. Eindhoven University of Technology, The Netherland; 2008.

[67] Hofmeyer H. An explicit, dynamic finite element model for the local failure of cold-formed trapezoidal sheeting. In: LaBoube Roger A, Yu Wei-Wen editors. Proceedings of the 21st international speciality conference on recent research and developments in cold-formed steel design and construction. St.-Louis, Missouri, USA. Department of Civil, Architectural and Environmental Engineering. Rolla, Missouri: Missouri University of Science and Technology; October 24 and 25 2012. p. 407–23.